

Asymmetric gear rectifies random robot motion

This article has been downloaded from IOPscience. Please scroll down to see the full text article.

2013 EPL 102 50007

(<http://iopscience.iop.org/0295-5075/102/5/50007>)

View [the table of contents for this issue](#), or go to the [journal homepage](#) for more

Download details:

IP Address: 202.120.52.1

The article was downloaded on 03/07/2013 at 01:40

Please note that [terms and conditions apply](#).

Asymmetric gear rectifies random robot motion

HE LI and H. P. ZHANG^(a)*Department of Physics and Institute of Natural Sciences, Shanghai Jiao Tong University
Shanghai, 200240, China*received 17 March 2013; accepted in final form 24 May 2013
published online 24 June 2013

PACS 05.70.Ln – Nonequilibrium and irreversible thermodynamics

PACS 45.70.-n – Granular systems

PACS 87.17.Jj – Cell locomotion, chemotaxis

Abstract – We experimentally study the dynamics of centimetric robots and their interactions with rotary gears through inelastic collisions. Under the impacts of self-propelled robots, a gear with symmetric teeth diffuses with no preferred direction of motion. An asymmetric gear, however, rectifies random motion of nearby robots which, in return, exert a torque on the gear and drive it into unidirectional motion. Rectification efficiency increases with the degree of gear asymmetry. Our work demonstrates that asymmetric environments can be used to rectify and extract energy from random motion of macroscopic self-propelled particles.

Copyright © EPLA, 2013

Random thermal motion can be rectified to do work in many natural and artificial apparatuses. Such a rectification phenomenon is related to the breaking of underlying time and spatial symmetries [1–3]. The former asymmetry can occur if the system is driven far from thermal equilibrium so that detailed balance is lost; the spatial asymmetry may be realized by an external forcing. For example, in a Brownian ratchet, microscopic particles move uni-directionally in a spatially asymmetric potential that is turned on/off periodically to keep the system away from equilibrium [4,5]. In the biological world, living organisms can take in and dissipate energy and, in the process, achieve active (self-propelled) motion [6]. Since active motion involves irreversible energy consumption, in such systems, the out-of-equilibrium condition is naturally satisfied and a broken spatial symmetry can lead to a rectification process as shown in previous studies [7–10] where asymmetric objects immersed in a bath of randomly swimming bacteria are shown to exhibit directed motion.

The idea to use symmetry breakings to rectify random motion has also been explored in macroscopic granular systems. The dissipative nature of inelastic collisions between grains leads to an automatic breakdown of time-reversal symmetry and the spatial asymmetry can be broken either by using a geometrically asymmetric object [11–16] or by using a geometrically symmetric object that is made of materials with different elastic properties [17–20]. Several theoretical and numerical models have been constructed to illustrate the dynamics and fluctuations of translational

and rotational granular motors [12–14,17,19,21]. On the experimental side, researchers have used *external* vibration to excite macroscopic particles, which move randomly mimicking microscopic Brownian particles; the excited particles were able to drive rotors [15], gears [16], and asymmetric ratchet [18].

Here, we explore the possibility of using spatial asymmetry to rectify active motion of *macroscopic* objects that are *self-propelled*. In our experiments, centimetric robots self-propel and interact with environment through inelastic collisions. When immersed in a group of robots, a rotary gear with symmetric teeth exhibits diffusive motion with no preferred direction but a unidirectional motion spontaneously emerges for gears with asymmetric teeth. We systematically investigate how robot density and gear geometry affect gear motion and robot dynamics.

Experiments. – Robots used in our experiments are commercially available toys Hexbug Nano [22], which are also called bristlebots [23]. Top and side views of a robot are shown in fig. 1(a). The robot body, 4.3 cm long and 1.2 cm wide, houses a 1.5 V button cell battery that drives a vibration motor. We use fresh batteries in each new experiment and run experiments for less than 20 minutes to prevent battery power degrading. The robot body is supported by twelve flexible legs that all bends slightly backwards. When turned on, the vibration motor sets the robot into forward hopping motion on a solid substrate, as shown by the movie S1.mp4¹ in the on-line supplementary

¹The movie S1.mp4 shows a robot hopping on a flat Styrofoam. The movie is recorded at 190 frames/s and played at 19 frames/s.

^(a)E-mail: hepeng_zhang@sjtu.edu.cn

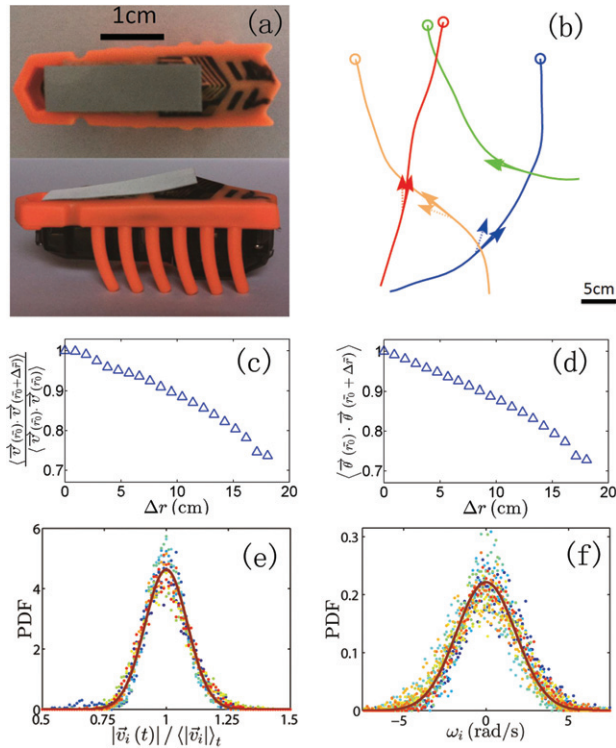


Fig. 1: (Color online) Dynamics of isolated individual robots. (a) Top and side views of a robot with a reflective sheet on the back. (b) Sample trajectories of isolated robots. Motion direction and body orientation of robots are shown by solid and dashed arrows, respectively. Velocity (c) and body orientation (d) correlation functions along trajectories of eleven isolated robots. Probability distribution of normalized translational speed (e) and angular velocity (f) measured in eleven isolated robots.

material. Quantitative mechanical models for such a hopping robot have been constructed in [23] and [24]; it has been demonstrated that the robot dynamics depends sensitively on the battery power, the robot mass, the elasticity of flexible legs, and the frictional property of the substrate.

An instantaneous configuration in a typical experiment is shown in fig. 2(a). Twenty robots move in an arena centered at O . The arena boundary, made of acrylic, is 2 cm tall (in the direction perpendicular to the page) and has a wavy shape. The wavy boundary effectively reduces the probability for robots to get stuck on the boundaries [25]. The bottom of the arena is made of a high-density (20 kg/m^3) Styrofoam sheet whose flat surface ensures the robot to move persistently forward.

Moving robots collide inelastically with a gear that can rotate freely around O . Both symmetric and asymmetric gears, shown in fig. 2(b), are used in our experiments. Geometry of a gear is determined by eight equally spaced exterior and interior vertices that lie on two concentric circles with radii of 8.5 cm and 11.5 cm. We systematically change gear geometry by varying the relative

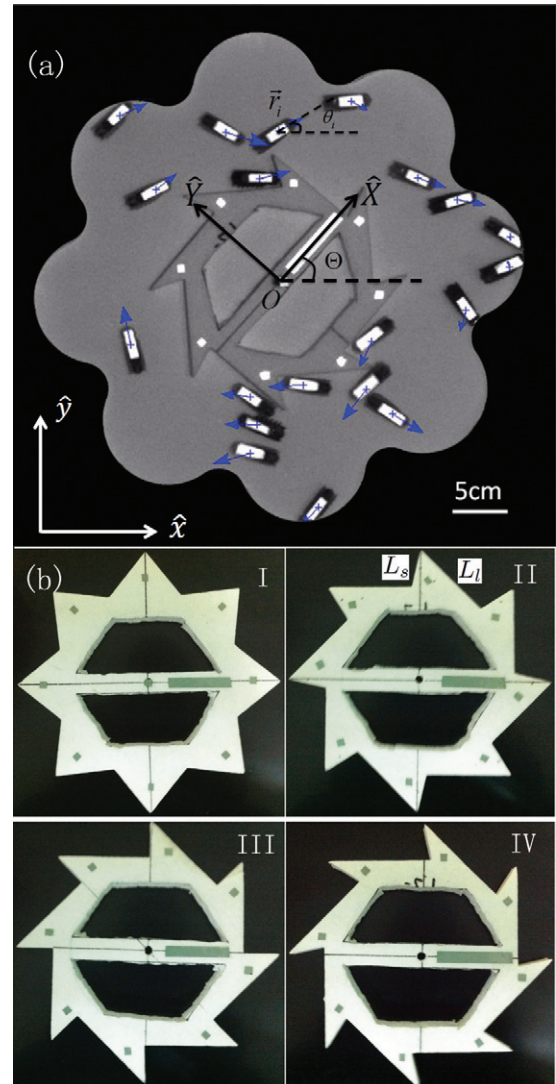


Fig. 2: (Color online) Experimental setup. (a) Twenty robots move in an arena with a curved boundary. A gear at the center of the arena is free to rotate (around point O) but not to translate. Reflective sheets are attached to robots and the gear to facilitate image analysis. Instantaneous robot translational velocities are extracted by a particle-tracking algorithm and shown by blue arrows. A stationary $(\hat{x}\hat{y})$ and a co-moving $(\hat{X}\hat{Y})$ coordinate frame are defined. (b) Four gears with different geometric parameters used in the experiments. Gears are numbered from Gear I to Gear IV. The length of the longer and shorter edges of a gear tooth are L_l and L_s , respectively.

angular separation between exterior and interior vertices. Quantitatively, we use the length of the longer and shorter edges of a gear tooth, L_l and L_s as defined in fig. 2(b), to describe a gear. When $L_l = L_s$, the gear is symmetric; otherwise, the gear is asymmetric. All gears are cut from a 2 cm thick Styrofoam sheet by a CNC foam cutter. Part of the interior material is removed to reduce the gear mass and each gear weighs around 8 g. The static friction coefficient between the gear and the substrate is 0.57 and

Table 1: Geometric parameters of four gears. The definitions of the parameters (L_l and L_s) are given in the text and in fig. 2(b).

	Gear I	Gear II	Gear III	Gear IV
L_l (cm)	5.5	7.5	8.2	8.8
L_s (cm)	5.5	3.4	3.2	3.2
$\chi = \frac{L_l}{L_s}$	1	2.2	2.6	2.7

the torque required to overcome the static friction and to set gears into motion is approximately $4.6 \times 10^{-3} \text{ N} \cdot \text{m}$. Detailed geometric parameters for four gears are shown in table 1.

We quantify gear and robot motion by imaging. To increase the contrast, reflective sheets are attached to robots and gears. Images are recorded by a CCD camera at a rate of 20 frames/s with a spatial resolution of $900 \times 900 \text{ pixel}^2$ over a field of view of $50 \times 50 \text{ cm}^2$. Images, compressed by MJPG codec to reduce the file size, are directly streamed to a hard disk for 1000 s periods, corresponding to 20000 images. From raw images, we use an analysis method based on intensity thresholding to extract position (center of mass) and orientation of the i -th robot at time t , denoted as $\vec{r}_i(t)$ and $\theta_i(t)$ in the stationary $\hat{x}\hat{y}$ frame, and gear orientation, $\Theta(t)$. Then a standard particle-tracking algorithm based on a minimum distance criterion is used to construct trajectories from the positions. From the trajectories, we derive instantaneous robot translational and rotational velocities as $\vec{v}_i = d(\vec{r}_i)/dt$, $\omega_i = d(\theta_i)/dt$, and the gear rotational velocity as $\Omega = d(\Theta)/dt$. In data analysis, velocities are computed as the discrete difference between two successive time steps. To better illustrate the mechanism of gear-robot interactions, we also define an $\hat{X}\hat{Y}$ coordinate frame co-moving with the gear, as shown in fig. 2(a).

Results. – We first examine the dynamics of an isolated robot. Four typical trajectories of isolated robots are plotted in fig. 1(b). These trajectories are collected in the central part of the arena to eliminate the effects of collisions between robots and the boundary; their length is limited. Robots mainly move in the direction of their body orientation as shown by solid and dashed arrows in panel (b). Trajectories consist of straight segments connected by random (but small) changes in motion direction. Robots can run persistently across the arena with small changes in their velocities and orientations. As shown in fig. 1(c), the inner product of the instantaneous robot velocities decreases approximately linearly as a function of separation and drops 30% of its value over 18 cm. A similar result is obtained for robot orientation as shown in fig. 1(d). We note that the spatial range over which the correlation functions in panels (c) and (d) can be measured is limited by the arena size.

The instantaneous translational speed of the i -th robot, $|\vec{v}_i(t)|$, fluctuates around its temporal mean $\langle |\vec{v}_i| \rangle_t$, where

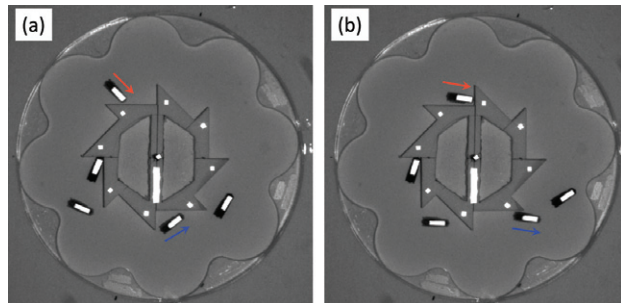


Fig. 3: (Color online). Asymmetric gear rectifies robot motion. Upon collision, the robot indicated by the red arrow aligns parallelly to the gear surface, slides towards the corner, gets stuck, and produces a clockwise torque on the gear. The other robot, indicated by the blue arrow, aligns along the surface after collision and moves back into the open space. Two frames are separated by 0.35 s in time.

$\langle \dots \rangle_t$ denotes an average over time. To quantify the speed fluctuations, probability distributions of $|\vec{v}_i(t)| / \langle |\vec{v}_i| \rangle_t$ for eleven robots are plotted in fig. 1(c) with a Gaussian fit; the speed averaged over all times and all robots is $V = \langle |\vec{v}_i| \rangle_{t,i} = 19.9 \text{ cm/s}$. Robots change their body orientations randomly and their angular velocities follow a Gaussian distribution centered at zero with a width of 1.8 rad/s, as shown in (d). Fluctuations in translation and rotation velocities may arise from manufacturing imperfection of robots and surface roughness of the arena bottom.

Robots interact with gears through inelastic collisions. In fig. 3(a), two robots, indicated by red and blue arrows, approach the gear with an incident angle of around 45 degrees. Upon collision, robots lose their velocity component normal to the gear surfaces and begin to slide along the surfaces; this leads to the accumulation of robots near the gears. To quantify this phenomenon, we compute a temporally averaged robot density in the co-moving frame $\hat{X}\hat{Y}$ (cf. fig. 1) as $\rho(X, Y) = \langle \sum_i \delta(X\hat{X} + Y\hat{Y} - \vec{R}_i(t)) \rangle_t$, where $\vec{R}_i(t)$ is the position of the i -th robot in the $\hat{X}\hat{Y}$ frame and δ is a Dirac function. In the left column of fig. 4, we plot the robot density, $\rho(X, Y)$, normalized by the mean density in the arena, ρ_0 . In all cases, robots are uniformly distributed in regions away from gears and show a higher density near gears. At corners, the robot density can be as high as four times the mean. We use up to thirty robots in our system and the area fraction occupied by thirty robots is 15%; such a density is much lower than that in Deseigne *et al.* [26], where spontaneous large scale collective motion was observed.

In the arena, robots mainly move azimuthally around O and the motion in the radial direction is limited by boundaries. We compute temporally averaged azimuthal velocity in the co-moving frame as $w(X, Y) = \frac{\langle \sum_i w_i(t) \delta(X\hat{X} + Y\hat{Y} - \vec{R}_i(t)) \rangle_t}{\rho(X, Y)}$, where $w_i(t)$ is the azimuthal velocity component of the i -th robot. If the gear is

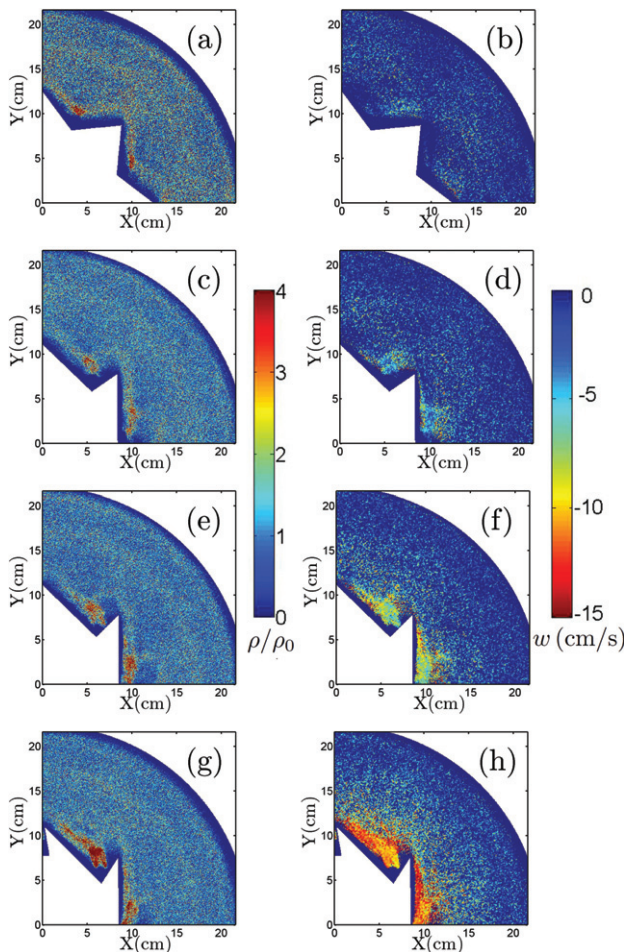


Fig. 4: (Color online) Temporally averaged robot density (left column) and robot azimuthal velocity (right column) in the first quadrant of the co-moving coordinate frame $\hat{X}\hat{Y}$ (defined in fig. 1). Results for the same type of gear are shown in a horizontal roll: (a) and (b) for Gear I; (c) and (d) for Gear II; (e) and (f) for Gear III; and (g) and (h) for Gear IV. Thirty robots are used in all experiments. We note that there is an excluded-volume region around the gear; the width of the region is approximately half the robot width (0.6 cm).

symmetric (S2.mp4²), two edges of a gear tooth have the same length. Robots have equal probabilities to collide with either one of the two edges and to move in the clockwise or counterclockwise directions. Consequently, $w(X, Y)$ is close to zero everywhere in the arena, as shown in fig. 4(b). This means that a symmetric gear cannot rectify the random robot motion and that there is an equal possibility for the gear to be pushed by robots in either direction, as shown by the probability distributions of the gear speed in fig. 5(a). Gear motion is further quantified by mean-square angular displacement, $\langle \Delta\theta^2(\Delta t) \rangle = \langle (\theta(t + \Delta t) - \theta(t))^2 \rangle_t$; red lines in fig. 5(b) show a diffusive behavior in the long-time limit: $\langle \Delta\theta^2(\Delta t) \rangle \propto t$.

²The movie S2.mp4 shows motion of a symmetric gear driven by thirty robots. A small portion of robots flips over during experiments; they usually can recover to a running state in a few seconds. The movie is recorded and played at 20 frames/s.

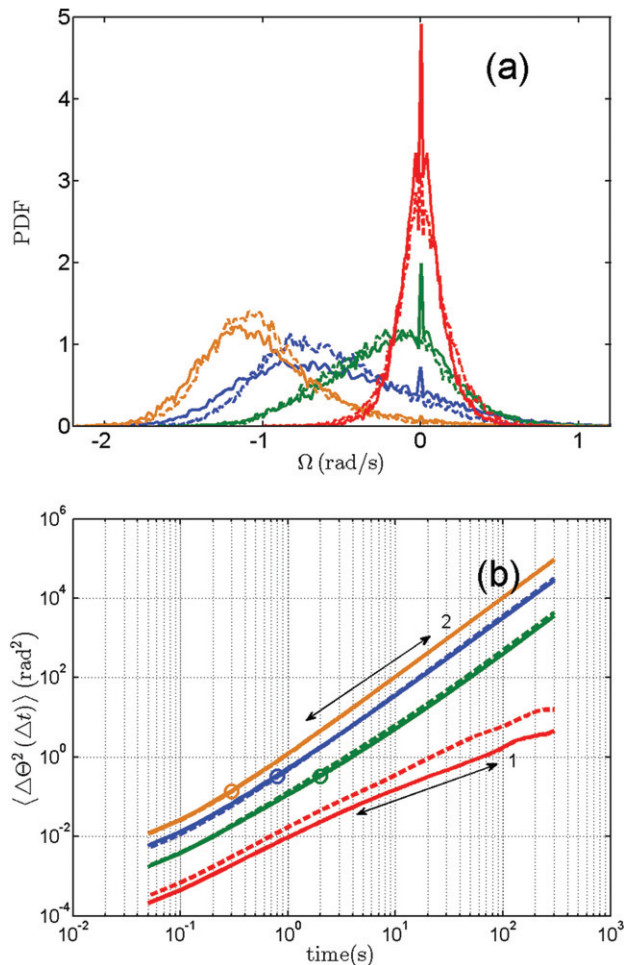


Fig. 5: (Color online) Dynamics of gears driven by robots. (a) Probability distribution of angular velocity for four gears; (b) angular mean-square displacement of four gears. Circles mark the beginning of the ballistic motion of asymmetric gears. Two black lines with slopes of 1 and 2 are shown for reference. Curves in both panels are color-coded: red for Gear I, green for Gear II, blue for Gear III, and yellow for Gear IV. Gears are driven by twenty (solid lines) or thirty (dashed lines) robots.

For asymmetric gears (S3.mp4, S4.mp4, and S5.mp4³), two edges of a gear tooth have different length. Robots have a higher probability to collide with and slide along longer edges. As shown in fig. 3, among the robots colliding with longer edges, those moving clockwise get stuck in the corner, while others leave the gear and move back to the open space [8,9]. This leads to more clockwise moving robots near the gear, therefore, to a non-zero mean robot velocity, $w(X, Y)$, as shown in the panels (d), (f), (h) in fig. 4. Robots in clockwise motion push on the shorter edge of the gear and create a net torque that drives the gear into directed motion. The probability distributions of gear rotational velocity Ω are

³Movies S3.mp4, S4.mp4, and S5.mp4 show the motion of asymmetric gears driven by thirty robots. A small portion of robots flips over during experiments; they usually can recover to a running state in a few seconds. The movie is recorded and played at 20 frames/s.

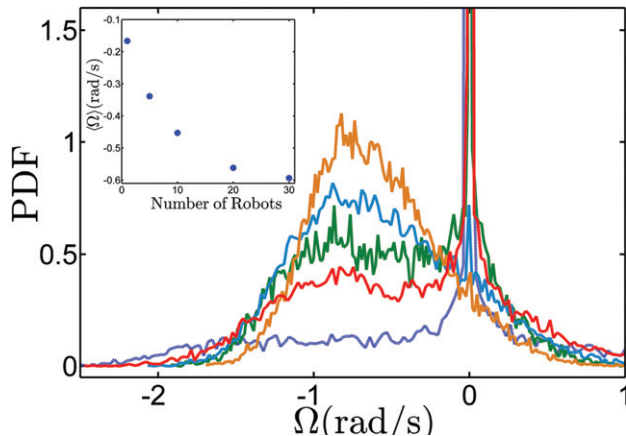


Fig. 6: (Color online). Probability distributions of gear velocity measured under five robot densities. Curves from the top to the bottom correspond to cases of 30, 20, 10, 5, 1 robots, respectively. The mean gear velocity is plotted as a function of the number of robots in the inset. Gear III is used in these measurements.

shown in fig. 5(a) for three asymmetric gears. Directed motion of asymmetric gears is also quantified by the mean-square displacements in fig. 5(b); in the long-time limit, asymmetric gears move ballistically: $\langle \Delta\theta^2(\Delta t) \rangle \propto t^2$.

The geometry of a gear has both qualitative and quantitative effects on its motion. Symmetric gear diffuses with no preferred direction for motion; asymmetric gears exhibit directed ballistic motion in the long-time limit. When the asymmetry is weak, $\chi = 2.2$, there is still significant chance for the gear to rotate in the counter-clockwise (positive) direction and the most probable value of Ω is zero, shown in fig. 5(a). As χ increases, the probability of positive Ω decreases and the most probable value of Ω shifts from zero to negative values. For the gear with $\chi = 2.7$, the probability for negative Ω becomes negligible and the most probable value of Ω is 1.3 rad/s, which means that the outer vertices of the gear move at a linear speed of 14.9 cm/s, comparable to the mean robot speed $V = 19.9$ cm/s. We note that distributions for asymmetric gears in fig. 5(a) are asymmetric with respect to their peaks and are different from those in the previous experimental study of a granular motor driven by externally excited grains [18]. The mean-square displacements of asymmetric gears in fig. 5(b) deviate from ballistic motion for small time separations as marked by circle symbols. As the asymmetry increases, the transition time decreases.

We systematically study the effects of a number of robots on gear motion. The frictional torque on gears is small enough so that it is possible for a single robot to move the gears. However, if the number of robots is too small, robots spend most of their time running freely and interact with the gears infrequently. This leads to a weak rectification effect: gears move intermittently with small mean velocity and probability distributions of gear

velocity peak sharply at zero, as shown by the data for the cases of 5 robots and 1 robot in fig. 6.

Discussion. – Rectified gear rotation has been previously demonstrated in bacterial systems [8–10]. Like robots in our experiments, bacteria tend to accumulate and move along solid boundaries; such boundary-following motility is likely caused by hydrodynamic interactions between bacteria and boundaries [8–10,27–29], which is different from the inelastic collisions in our system. Despite the differences in microscopic origin, boundary-following motility leads to rectified behaviors in two systems that have very different lengthscales. This suggests that one can use boundary-following motility as a general method to rectify random motion [7].

Macroscopic experimental systems capable of rectifying random motion have been reported before [15,16,18]. In these experiments, grains were globally excited through vertical vibrations produced by a shaker and vibration systems have to be carefully balanced to achieve a uniform forcing. In contrast, robots in our experiments are self-propelled and we can achieve a uniform excitation (as shown in fig. 4) with relative low costs and experimental complexities. Another advantage of a self-propelled system is that it allows independent tuning of individual robot motility. In a broader scope, a self-propelled system may be used to study a wide range of phenomena that have been investigated by excited granular systems, such as collective motion [30], glass transition [31], and polymer dynamics [32].

In conclusion, we have investigated the dynamics of self-propelled robots and their interactions with rotary gears. Robots are internally driven and move mainly along their body direction with fluctuations in both velocity magnitude and direction. Inelastic collisions between robots and gears lead to the accumulation of robots around gears. Random motion of accumulated robots is rectified by asymmetric gears. Rectified robot motion, in response, drives asymmetric gears into directed motion. Rectification efficiency increases with the degree of gear asymmetry.

We thank YUN ZHANG for his help in the early stage of the project. HPZ acknowledges financial support of the National Natural Science Foundation of China through Grant No. 11104179, of the Shanghai Pujiang Program through Grant No. 12PJ1405400, and of The Program for Professor of Special Appointment (Eastern Scholar) at Shanghai Institutions of Higher Learning through Grant No. SHDP201301.

REFERENCES

- [1] ASTUMIAN R. D. and HÄNGGI P., *Phys. Today* **55**, issue No. 11 (2002) 33.

-
- [2] REIMANN P., *Phys. Rep.*, **361** (2002) 57.
- [3] HÄNGGI P. and MARCHESONI F., *Rev. Mod. Phys.*, **81** (2009) 387.
- [4] ROUSSELET J., SALOME L., AJDARI A. and PROST J., *Nature*, **370** (1994) 446.
- [5] FAUCHEUX L. P., BOURDIEU L. S., KAPLAN P. D. and LIBCHABER A. J., *Phys. Rev. Lett.*, **74** (1995) 1504.
- [6] RAMASWAMY S., *Annu. Rev. Condens. Matter Phys.*, **1** (2010) 323.
- [7] GALAJDA P., KEYMER J., CHAIKIN P. and AUSTIN R., *J. Bacteriol.*, **189** (2007) 8704.
- [8] ANGELANI L., DI LEONARDO R. and RUOCCO G., *Phys. Rev. Lett.*, **102** (2009) 048104.
- [9] DI LEONARDO R., ANGELANI L., DELL'ARCIPRETE D., RUOCCO G., IEBBA V., SCHIPPA S., CONTE M. P., MECARINI F., DE ANGELIS F. and DI FABRIZIO E., *Proc. Natl. Acad. Sci. U.S.A.*, **107** (2010) 9541.
- [10] SOKOLOV A., APODACA M. M., GRZYBOWSKI B. A. and ARANSON I. S., *Proc. Nat. Acad. Sci. U.S.A.*, **107** (2010) 969.
- [11] FARKAS Z., TEGZES P., VUKICS A. and VICSEK T., *Phys. Rev. E*, **60** (1999) 7022.
- [12] CLEUREN B. and VAN DEN BROECK C., *EPL*, **77** (2007) 50003.
- [13] COSTANTINI G., MARCONI U. M. B. and PUGLISI A., *Phys. Rev. E*, **75** (2007) 061124.
- [14] CLEUREN B. and EICHHORN R., *J. Stat. Mech.: Theory Exp.* (2008) P10011.
- [15] BALZAN R., DALTON F., LORETO V., PETRI A. and PONTUALE G., *Phys. Rev. E*, **83** (2011) 031310.
- [16] HECKEL M., MÜLLER P., PÖSCHEL T. and GALLAS J. A. C., *Phys. Rev. E*, **86** (2012) 061310.
- [17] COSTANTINI G., MARCONI U. M. B. and PUGLISI A., *EPL*, **82** (2008) 50008.
- [18] ESHUIS P., VAN DER WEELE K., LOHSE D. and VAN DER MEER D., *Phys. Rev. Lett.*, **104** (2010) 248001.
- [19] TALBOT J., WILDMAN R. D. and VIOT P., *Phys. Rev. Lett.*, **107** (2011) 138001.
- [20] TALBOT J. and VIOT P., *Phys. Rev. E*, **85** (2012) 021310.
- [21] PIASECKI J., TALBOT J. and VIOT P., *Phys. Rev. E*, **75** (2007) 051307.
- [22] <http://www.hexbug.com/nano/>.
- [23] GIOMI L., HAWLEY-WELD N. and MAHADEVAN L., *Proc. R. Soc. A: Math. Phys. Eng. Sci.*, **469** (2013) 20120637.
- [24] DESIMONE A. and TATONE A., *Eur. Phys. J. E*, **35** (2012) 1.
- [25] DESEIGNE J., DAUCHOT O. and CHATE H., *Phys. Rev. Lett.*, **105** (2010) 098001.
- [26] DESEIGNE J., LEONARD S., DAUCHOT O. and CHATE H., *Soft Matter*, **8** (2012) 5629.
- [27] BERKE A. P., TURNER L., BERG H. C. and LAUGA E., *Phys. Rev. Lett.*, **101** (2008) 038102.
- [28] LI G. L. and TANG J. X., *Phys. Rev. Lett.*, **103** (2009) 078101.
- [29] SPAGNOLIE S. E. and LAUGA E., *J. Fluid Mech.*, **700** (2012) 105.
- [30] NARAYAN V., RAMASWAMY S. and MENON N., *Science*, **317** (2007) 105.
- [31] REIS P. M., INGALE R. A. and SHATTUCK M. D., *Phys. Rev. Lett.*, **98** (2007) 188301.
- [32] SAFFORD K., KANTOR Y., KARDAR M. and KUDROLI A., *Phys. Rev. E*, **79** (2009) 061304.